Materials Today Chemistry 54 (2026) 103611

Contents lists available at ScienceDirect

Materials Today Chemistry

journal homepage: www.journals.elsevier.com/materials-today-chemistry/

Facile coating of floating polyurethane foams using reduced graphene oxide and TiO_2 for pollutant adsorption and photodegradation in water

Anna Dotti [a], Andrea Basso Peressut [a,*], Lorenzo Viganò [b], Barbara Di Credico [b], Roberto Matarrese [c], Saverio Latorrata [a]

[a] Department of Chemistry, Materials and Chemical Engineering "Giulio Natta", Politecnico di Milano, Piazza Leonardo da Vinci 32, 20133, Milano, Italy
[b] Department of Materials Science, INSTM, University of Milano-Bicocca, Via R. Cozzi 55, 20125, Milano, Italy
[c] Laboratory of Catalysis and Catalytic Processes, Department of Energy, Politecnico di Milano, Via La Masa 34, 20156, Milano, Italy

ARTICLE INFO

Keywords:
Reduced graphene oxide
Titanium dioxide
Photocatalysis
Water treatment
Rhodamine B

ABSTRACT

Developing effective and sustainable technologies for wastewater treatment is challenging in materials engineering. Photocatalysis based on TiO_2 is a promising solution for removing organic contaminants. However, the large bandgap and predominant use of TiO_2 nanoparticles hinder the industrial scalability of the process owing to the requirement of UV light, recovery issues, and potential environmental concerns. This study developed a simple and low-energy consuming strategy to combine TiO_2 nanopowder and reduced graphene oxide (rGO) in a water-based coating for polyurethane (PU) foams. The addition of rGO provides multiple synergistic functions including (i) immobilization of TiO_2 particles, (ii) adsorption of organic pollutants, improving the contact with catalytic sites, and (iii) partial bandgap narrowing, as reported in the literature. Commercial PU foams (20 PPI; 5.5 cm diameter; 0.5 cm thickness) were dip-coated with formulations at rGO:TiO_2 mass ratios of 1:1, 1:2, and 1:3. Photocatalytic activity was assessed via Rhodamine B (RhB) degradation (3 mg L^{-1} aqueous solution) under UV-Vis irradiation. Complete removal was achieved within 90 min by using rGO-TiO_2 1:3-coated samples, as evidenced by the subsequent RhB release experiments. Coated foams were fully characterized, both before and after decontamination tests, through thermal (TG and DSC), spectroscopic (EDX, UV-Vis, and ICP-OES) and morphological (optical microscopy and SEM) analyses, which confirmed coating stability. The proposed binder-free strategy provides a scalable route to design multifunctional photocatalytic foams. Moreover, by bridging materials engineering with environmental applications, it opens perspectives for the development of sustainable, easily deployable wastewater treatment systems.

1. Introduction

Various types of contaminants, ranging from inorganic (e.g., heavy metals) to organic (e.g., drugs, dyes, microplastics) materials, pollute wastewater and are a pressing concern worldwide, requiring the development of efficient and cost-effective decontamination technologies. Adsorption is a popular water treatment solution because of its versatility, simplicity, and low cost. However, it has proven low efficacy towards the removal of organic pollutants in aquatic environments [1].

Photocatalysis is a sustainable alternative for water decontamination from organic molecules. Upon light absorption, photo-generated electrons and holes are separated into the conduction and valence bands, respectively, of photocatalytic materials. This process enables highly reactive species (i.e., $HO^{\bullet}$ and $O_2^{\bullet -}$), produced by the reaction with O_2 and H_2O, to degrade organic contaminants, converting them into less or non-harmful compounds. In principle, photocatalysts can be reused multiple times and are effective toward a broad range of contaminants [2]. TiO_2 is the most studied and used photocatalyst [3], [4], [5] and is stable, non-toxic, relatively inexpensive, and easy to produce at an industrial scale [6]. Nevertheless, its practical application is still limited because of two main reasons. First, TiO_2 has a bandgap of 3.2 eV; therefore, TiO_2-mediated photocatalysis occurs only under UV light, leading to significant energy consumption [7], [8]. Second, TiO_2 is mainly used in slurry reactors in the form of nanoparticles, which tend to agglomerate, thereby significantly reducing the photocatalytic efficiency [9], [10]. Furthermore, safely and completely recovering the

* Corresponding author.
E-mail addresses: anna.dotti@polimi.it (A. Dotti), andreastefano.basso@polimi.it (A. Basso Peressut), l.vigano22@campus.unimib.it (L. Viganò), barbara.dicredico@unimib.it (B. Di Credico), roberto.matarrese@polimi.it (R. Matarrese), saverio.latorrata@polimi.it (S. Latorrata).

https://doi.org/10.1016/j.mtchem.2026.103611
Received 24 June 2025; Received in revised form 13 March 2026; Accepted 11 April 2026
Available online 16 April 2026

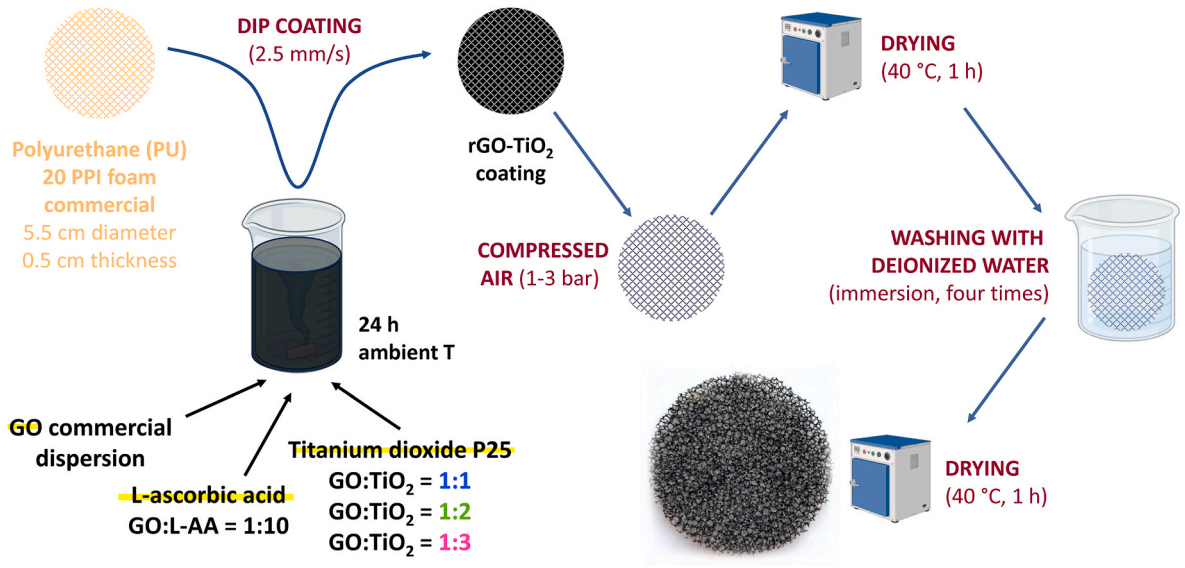

Fig. 1. Foam-coating procedure.

TiO_2 nanopowder is difficult, leading to significant risks of dispersion in the environment [11], [12].

Integrating TiO_2 with graphene oxide (GO), particularly in its reduced form (rGO), can provide several advantages [13], [14]. GO is similar to graphene with an alternated sp^2/sp^3 carbon network structure bearing hydroxyl, epoxy, and carboxyl groups. Although the number of functional groups in rGO is reduced upon controlled reduction, they are sufficient to impart self-assembling properties to the material [15]. This feature can be exploited for the development of macrostructures containing immobilized titania nanoparticles, such as the composite self-standing membrane recently developed by Basso Peressut et al. [16]. Embedded in self-assembled structures, TiO_2 particles do not agglomerate and can be easily handled and safely recovered from water. The presence of rGO can also improve TiO_2 decontamination performance. Owing to its excellent adsorption properties toward both metal ions and organic molecules [17], [18], rGO can capture contaminants and keep them in direct contact with the photocatalyst, thereby favoring the degradation of the organic fraction if properly irradiated [19], [20]. Moreover, rGO-TiO_2 composites have a lower bandgap than pure TiO_2, thereby enabling visible and solar light-driven photocatalysis [21], [22], [23], [24]. The presence of rGO can also increase the photocatalytic efficiency, as it was reported to improve the separation of photo-generated charge carriers [24], [25], [26], [27], [28], [29].

Different types of substrates have been employed for the deposition of reduced GO-TiO_2 composites. Two dimensional (2D) supports including polymeric membranes [30], [31], [32], [33], cellulose membranes [34], glass [35], as well as cotton and polyamide textiles [36], and three-dimensional (3D) scaffolds such as ceramic monoliths [37], optical fibers [38], and melamine sponges [39] have been used. Among the 3D structures, polyurethane (PU) foams are recognized as a conventional material for water treatment applications because of their open-pore structure, low cost, commercial availability, easy handling, and low density, which enable them to float in water [40], [41]. Multiple structures consisting of PU foams modified with GO or rGO have been employed for the adsorption of various types of contaminants [41], [42], [43], [44]. TiO_2-functionalization of PU foams surface has recently garnered interest because the photocatalytic properties of TiO_2 can be enhanced when it is deposited on a floating support [45], [46], [47], [48], [49]. Nevertheless, the deposition of both rGO and TiO_2 on PU foams has not been significantly explored yet [50], [51].

This study exploited the self-assembling properties of rGO to coat commercial PU floating foams with a binder-free coating of rGO and TiO_2 nanopowder by considering several mass ratios between rGO and TiO_2. Although other TiO_2 and graphene-based photocatalytic foams can be found in the literature [52], [53], [54], [55], [56], their preparation requires the use of toxic reagents and complex synthetic procedures. Conversely, this study aimed to demonstrate the feasibility of a facile coating procedure for the deposition of rGO and TiO_2 on PU foams. The simple and low-energy consuming strategy proposed in this study is based on i) the reduction of GO at room temperature and pressure, ii) dip coating and blowing of compressed air, iii) drying at 40 °C. In addition, instead of the commonly used hydrazine, L-ascorbic acid was employed as an eco-friendly reducing agent. Samples were characterized via thermogravimetric (TG) and differential scanning calorimetry (DSC) analyses, optical microscopy, and scanning electron microscopy coupled with energy-dispersive X-ray (SEM-EDX) spectroscopy. Coated foams were subjected to adsorption and photodegradation tests using a 3 mg L^{-1} Rhodamine B (RhB) aqueous solution as a model organic pollutant [57], [58], [59]. After the foams were subjected to decontamination tests, they were observed under a 366-nm light to verify the presence of the adsorbed dye. Finally, the possible release of RhB was assessed by immersing the foams in deionized water (dH_2O). Preliminary RhB removal experiments were performed to demonstrate the potential application of these materials for water decontamination.

2. Materials and methods

2.1. Material preparation

First, a 4 mg mL^{-1} commercial aqueous dispersion of GO, purchased from Graphenea, was chemically reduced by stirring at ambient temperature (i.e., 20–25 °C) for 24 h via an eco-friendly process involving L-ascorbic acid (L-AA) (Sigma Aldrich) at an L-AA:GO mass ratio of 10:1, as shown in Fig. 1. Subsequently, TiO_2 nanopowder (Degussa P25, Sigma Aldrich) was introduced in the last 30 min of the reduction process at GO:TiO_2 mass ratios of 1:1, 1:2, and 1:3. A dispersion containing only rGO, without TiO_2, was also prepared for reference purposes. A commercial PU foam of 20 pores per inch (PPI), provided by Modulor as a 0.5-cm-thick foil, was manually cut into cylinders with a diameter of 5.5 cm. The resulting samples, without any preliminary treatment, were dip coated with rGO, rGO:TiO_2 1:1, 1:2, or 1:3 dispersions. Both immersion and extraction velocities were set to 2.5 mm s^{-1} on a custom-made dip coater. The immersion time was 30 s. Subsequently, the excess coating deposited in the foam pores was removed using

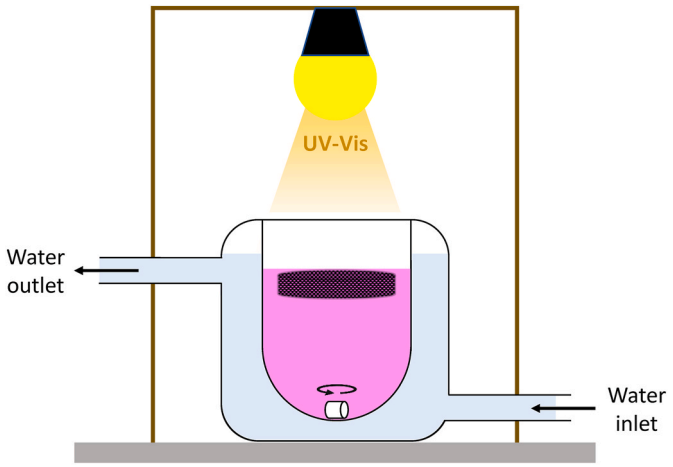

Fig. 2. Schematic of the batch photoreactor.

compressed air at a pressure of 1 to 3 bar. The samples were then dried at 40 °C for 1 h in an oven. To remove the excess L-AA, each foam sample was immersed four times in 300 mL of dH_2O for 10 min under static conditions. Finally, the samples were dried at 40 °C for 1 h and were weighed before and after the coating procedure to determine the amount of deposited material. The results presented here denote the average weight of seven samples along with the corresponding standard deviation.

2.2. Material characterization

2.2.1. Characterization techniques

Pristine and coated PU foams were observed under an optical microscope (Olympus sz-40) at 10x magnification. SEM-EDX analysis was performed using a Zeiss EVO 50 EP scanning electron microscope combined with an Oxford INCA energy 2000 spectrometer operated under high vacuum (10^{-5}–10^{-6} torr), at 20 kV, and with a probe current of 120 pA. The PU samples were sputtered with gold before the analysis. SEM images and EDX elemental maps were acquired at 100x magnification. TG analyses (TGA) were conducted using a Discovery TGA 550 equipment (TA Instruments) in nitrogen atmosphere (40 mL min^{-1} flux) at a heating rate of 10 °C min^{-1} from room temperature to 800 °C. DSC was performed using a Mettler-Toledo DSC 823e instrument between −60 °C and 200 °C. The experiments comprised three ramp cycles: heating, cooling, and heating, with both heating and cooling rates set to 20 °C min^{-1}. The thermal transitions of PU and their corresponding temperatures were determined by analyzing the third ramp cycle.

2.2.2. Coating stability test

To qualitatively evaluate the coating stability on the PU foam, the samples were immersed in dH_2O and ultrasonicated (Labsonic LBS1-6, Falc Instruments) for 30 min. Subsequently, the foams were dried in an oven at 40 °C for 1 h. The mass percentage of the coating detached from the substrate (CL_{US}) was calculated according to Equation (1):

$$CL_{US} = \frac{mcl_{us}}{mc} \times 100 \quad (1)$$

where mcl_{us} is the mass of the coating lost during the stability test and mc is the mass of coating at the end of the washing cycles.

2.3. Water decontamination

Photocatalytic experiments with RhB were conducted in a water-cooled reactor to maintain the solution temperature throughout the experiment between 20 °C and 25 °C, as measured by a thermocouple. Each floating foam sample was contacted with 100 mL of a 3 mg L^{-1} RhB (Sigma Aldrich) aqueous solution. Mild magnetic stirring was applied to guarantee the homogeneity of the reaction mixture. A 300 W UV-Vis Osram Ultra Vitalux lamp was used as a light source. The lamp was positioned 14 cm above the solution free surface, i.e., above the floating foam, and the lamp emission, measured using a light meter HD2302.0 (Delta OHM), was approximately 1200 W m^{-2} over its entire spectrum, of which around 35 W m^{-2} was in the UVA region and 10 W m^{-2} in the UVB region. A schematic of the experimental setup is shown in Fig. 2. Prior to irradiation, the suspension was kept in the dark for 30 min. Solution samples were withdrawn at fixed times, and the evolution of RhB concentration was monitored via UV-Vis spectroscopy (Cary 5000, Jasco) by monitoring the absorption peak at 554 nm. The photolytic degradation of RhB as well as the adsorption experiments in the dark were performed using the same experimental setup.

All experiments were performed in triplicate, and the results are reported as the average values along with the corresponding standard deviations.

To qualitatively assess RhB retention on the foam samples after adsorption and photodegradation tests, they were observed under illumination using a 366 nm lamp.

Ti leaching into the solution was investigated using inductively coupled plasma optical emission spectroscopy (ICP-OES) (PerkinElmer Optima 3000 SD). The analyses were performed both on the RhB solutions collected at the end of the adsorption and photodegradation experiments with rGO:TiO_2 1:3-coated samples and on 100 mL of dH_2O, in which the same samples had been immersed under static conditions for 72 h.

RhB release tests were performed by immersing each foam sample previously used in the water decontamination experiments in 100 mL of dH_2O under static conditions. Aliquots were withdrawn at fixed times, and RhB release was determined via UV-Vis spectroscopy by monitoring the absorption peak at 554 nm.

3. Results and discussion

3.1. Foam coating and characterization

The complete characterization of the coating constituents, i.e., rGO and TiO_2, has been reported in previous studies [16], [17].

Regarding rGO, the analysis of X-ray diffraction (XRD) plots and Fourier-transform infrared (FT-IR) spectra confirms the partial reduction of GO. The XRD plots exhibit the typical GO reflection at approximately 11° 2θ along with a shoulder at roughly 22° 2θ, corresponding to the formation of partially reduced domains [16]. The FT-IR spectra support this interpretation by showing a decrease in the intensity of the absorption bands between 900 and 1400 cm^{-1}, which is assigned to the original oxygen-bearing moieties of GO, especially the one corresponding to the stretching mode of epoxy groups (approximately 1300 cm^{-1}) [17]. Similarly, the Raman spectra of rGO display sharpened D and G bands with respect to virgin GO, an increased intensity in the second order 2D and D + G modes, and a decrease in the D/G intensity ratio (from 2.4 in GO to 2.1 in rGO) [17]. UV-Vis diffuse reflectance spectra (DRS) demonstrate the strong absorption behavior of rGO over both UV and visible ranges; this is because of the restored π-conjugated structure of the basal plane following the reduction process [16].

Regarding pure TiO_2, the XRD plots confirm the presence of both anatase (the major phase accounting for approximately 83%) and rutile phases. The photoactive phase (i.e., anatase) is also responsible for the appearance of four Raman peaks in the 140–640 cm^{-1} range [16]. The UV-Vis DRS show the characteristic absorption edge of TiO_2 at nearly 400 nm, corresponding to a bandgap of approximately 3.25 eV, as calculated using the transformed Kubelka–Munk function [16]. The combination of TiO_2 with rGO enhanced UV light absorption and caused a slight redshift of the absorption edge of rGO, which may provide a better utilization of the entire UV-Vis spectrum for photodegradation applications [16].

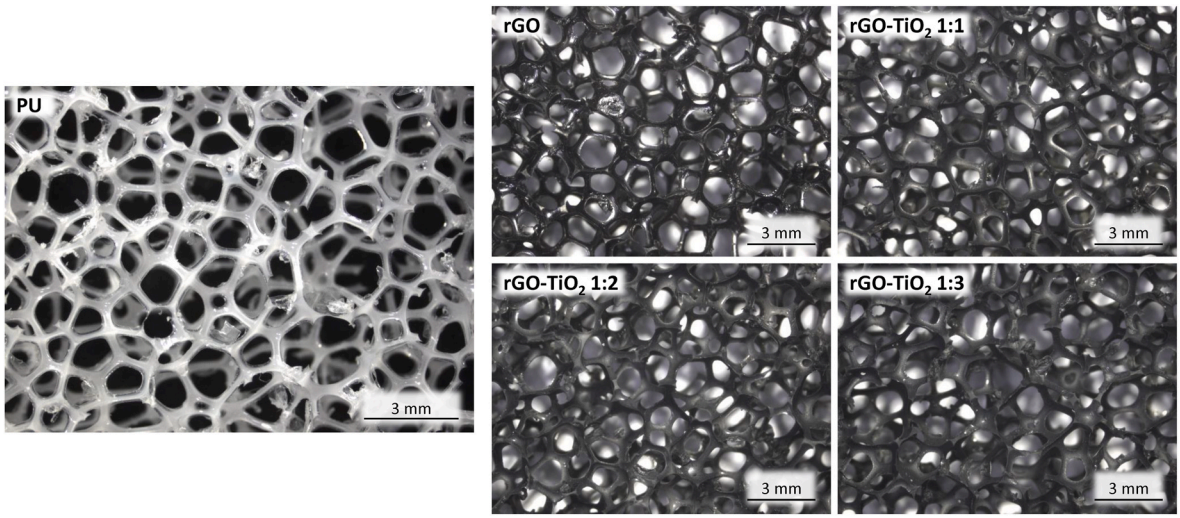

Fig. 3. Optical microscopy images of pristine PU (left) and coated (right) foam samples at 10x magnification.

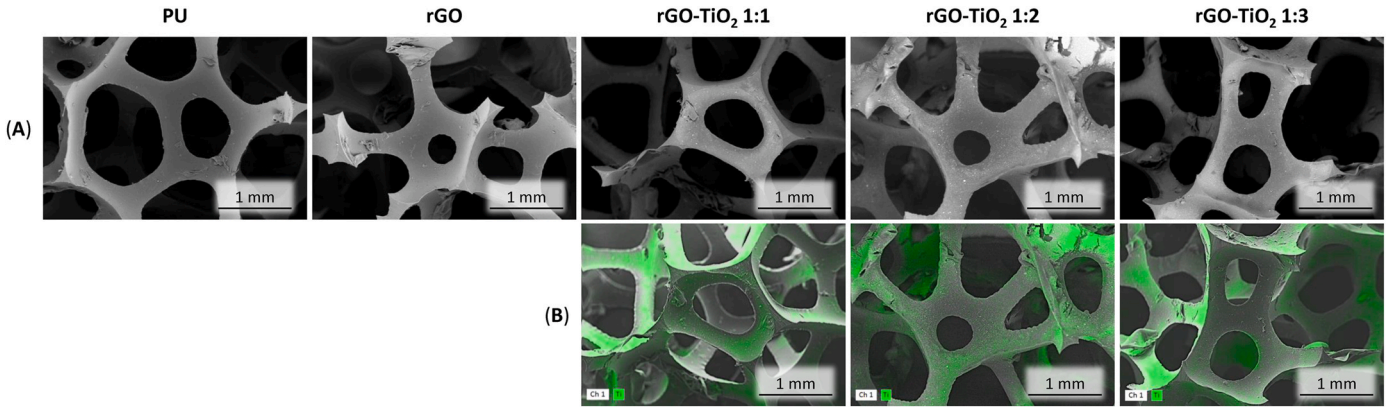

Fig. 4. SEM images with backscattered electrons (A) and EDX probes (B) of pristine PU, rGO-, rGO-TiO_2 1:1-, 1:2-, and 1:3-coated foams at 100x magnification.

Table 1
Average foam weights after coating and the corresponding average mass of the coating.

Coating type	Coated foam weight (mg)	Coating mass (mg)
rGO	325.3 ± 3.5	6.9 ± 0.6
rGO-TiO_2 1:1	341.3 ± 6.3	11.4 ± 1.2
rGO-TiO_2 1:2	348.6 ± 5.7	16.4 ± 0.9
rGO-TiO_2 1:3	346.9 ± 5.5	18.9 ± 0.7

The foam samples were coated under mild conditions using a simple procedure. Pristine PU foams were manually cut into cylinders of 5.5 cm diameter and 0.5 cm thickness, which weighed approximately 320 mg. Optical microscopy images show the PU foam macrostructures (Fig. 3) consisting of irregular pores with diameters ranging from hundreds of micrometers to a few millimeters. After the coating and washing processes, the color of the foam samples changed from white (typical of pristine PU) to black (typical of rGO). With the introduction of titania, the coatings appeared more opaque and less reflecting compared to those containing only rGO. Optical microscopy images also confirmed the effectiveness of employing compressed air to remove the excess coating as the majority of pores was not occluded.

SEM images (Fig. 4) further highlight the irregularity of the foam structure. Backscattered electron (BSE) images (Fig. 4A) reveal that the TiO_2-containing foams exhibit many bright spots on their surface, corresponding to the TiO_2 particles encapsulated within the coating. SEM-EDX elemental maps (Fig. 4B) confirm a uniform distribution of Ti, indicating the presence of TiO_2 on 1:1, 1:2, and 1:3-coated samples.

As reported in Table 1, the average coating mass per sample was 6.9 mg for rGO. Introducing TiO_2 in a 1:1 mass ratio with respect to rGO almost doubled the amount of the deposited coating (11.4 mg), further suggesting the successful deposition of TiO_2 onto the foam. The mass increase was proportional for the 1:2-coated sample (16.9 mg), whereas it was smaller than the expected value for the 1:3-coated sample (18.9 mg). This may suggest that the increase in the deposited mass from plain rGO to rGO-TiO_2 1:1, 1:2, and 1:3 is influenced by other factors, such as the interaction among foam, rGO, and TiO_2, as well as the possible coating embrittlement following TiO_2 incorporation, in addition to the increase in the TiO_2 content in the coating formulation.

The thermal behavior of pristine and coated PU foams was investigated via TG (Fig. 5) to verify the possible effects of coating deposition on the original properties of PU.

The virgin polymer was characterized by a set of three overlapped thermal phenomena, unfolding in the 200–450 °C range and leading to the complete decomposition of the material (Fig. 5) [60], [61], [62]. These phenomena can be generally ascribed to the thermal cleavage of the hard segments of the PU matrix, such as urethane/urea bonds and chain extenders, followed by the scission of soft ones, i.e., the polyol segments of the polymer chains [61], [62], [63]. However, the exact attribution of each phenomenon to the different contributions of the DTG curve of PU (Fig. 5B) is not trivial. In fact, the complicated degradation mechanism of PU is strongly influenced by chemical

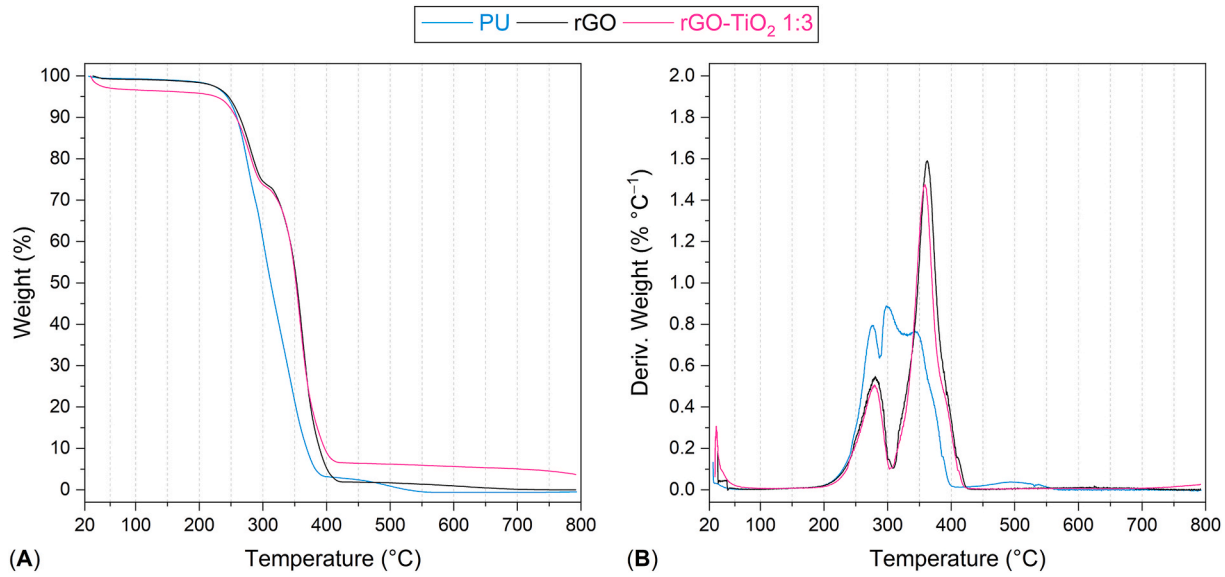

Fig. 5. TGA (A) and DTG (B) plots of pristine PU, rGO-coated, and rGO-TiO_2 1:3-coated foams.

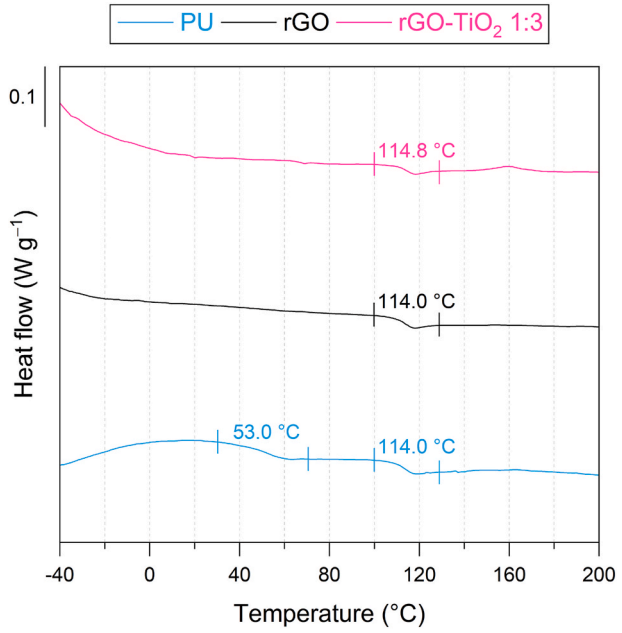

Fig. 6. Third ramp cycle of the DSC curves of pristine PU, rGO-coated, and rGO-TiO_2 1:3-coated foam samples.

composition, structure, and molecular weight of its hard and soft segments, as well as by their ratio in the polymer [63], [64]. According to the literature, the degradation of the hard segments of PU occurs at approximately 250–350 °C, whereas the soft segments are usually expected to decompose at higher temperatures (approximately 350–500 °C) [60], [61], [62], [63], [64].

The typical thermal events of rGO involve the evaporation of adsorbed water (up to 150 °C), degradation of the residual oxygen-bearing groups in the graphitic network after the reduction process (between 150 °C and 250 °C), and the decomposition of the basal planes (above 600 °C) [16]. Because of the low weight of the deposited coating with respect to the total weight of the foam (Table 1), these thermal phenomena cannot be discerned in the thermograms shown in Fig. 5. Conversely, TiO_2 did not exhibit thermal degradation in the analyzed temperature range [16], and its presence in the coating may be inferred from the higher residual weight of the rGO-TiO_2 1:3-coated specimen at 800 °C, i.e., approximately 3.6% (Fig. 5), with respect to both pristine and rGO-coated samples, which were completely decomposed at the same temperature.

When comparing the trends of the TG and DTG curves of bare and coated PU foams, a different distribution of the thermal phenomena can be observed between 200 °C and 450 °C (Fig. 5). Coated PU foams exhibited a more marked distinction between the degradation events occurring below or above 300 °C. However, the difference in their behavior was not caused by the contact of the foam with the coating, but rather by the exposure of the foam to heating in the oven. Fig. S1 (provided in Supplementary Information (SI)) shows a thermogram of an uncoated PU sample subjected to the same heating conditions of the rGO- and rGO-TiO_2 1:3-coated specimens, which were exposed to a temperature of 40 °C in an oven to consolidate the coating. Evidently, both heated PU (PU oven in Fig. S1) and rGO-/rGO-TiO_2 1:3-coated foams (Fig. 5) were characterized by equivalent thermograms, strengthening the hypothesis of a heat-induced modification of the original properties of PU.

The previous hypothesis is supported by the results of DSC analyses (Fig. 6 and S2). The third ramp/heating cycle of the DSC curve of bare PU enabled the identification of two thermal events at approximately 53 °C and 114 °C (Fig. 6).

The first thermal event occurred approximately between 30 °C and 70 °C, but it disappeared in both coated specimens (Fig. 6) and PU sample heated in the oven prior to the DSC analysis (Fig. S2). Thus, as the oven temperature (i.e., 40 °C) was within the range of the first thermal phenomenon (i.e., 30–70 °C), it can be hypothesized that heating the foam in the oven induces a permanent change in the original PU structure; this also explains the previously discussed change in the thermogram shape (Fig. 5 and S1).

Conversely, after the heat treatment in the oven, all foams exhibited a thermal phenomenon at a temperature of approximately 114 ± 1 °C, which is identified as the glass transition temperature (T_g) owing to its reversible nature. According to both calculations and literature data, the corresponding temperature range corresponds to the motion of the hard segments of the PU chains [65], [66]. This finding is compatible with the analysis of the TG curves (Fig. 5A), in which most thermal phenomena occurred below 400 °C, i.e., in a temperature range typically assigned to the decomposition of hard segments [60], [61], [62], [63], [64]. Contrarily, a higher content of soft segments could decrease the T_g even below 0 °C [65], [66]. However, as previously discussed, an accurate

Table 2
Mass percentage of coating loss during ultrasound stability tests.

Coating type	CL_{us}
rGO	10.8 ± 0.3%
rGO-TiO_2 1:1	9.1 ± 2.0%
rGO-TiO_2 1:2	10.8 ± 1.1%
rGO-TiO_2 1:3	12.7 ± 0.6%

comparison with the other PU types reported in the literature is not possible. This is because the properties (molecular structure and weight) of the hard and soft segments, as well as their ratios in the polymer and the percentage of recycled material in the formulation, strongly influence the resulting thermal behavior of PU, leading to a wide range of T_g values [65], [66], [67], [68].

Similarly to TG results, the DSC curves of the heated PU (PU oven in Fig. S2) and rGO-/rGO-TiO_2 1:3-coated foams (Fig. 6) are also equivalent. This indicates that the coating did not have detrimental interactions with the PU substrate, which was only affected by the oven-heating process. Notably, these slight modifications to the thermal behavior did not deteriorate the structural stability of the PU foam and did not impair its use as support for the photocatalytic coating.

3.1.1. Ultrasound stability test

To qualitatively assess the coating stability, the coated foam samples were subjected to ultrasound testing for 30 min under conditions that were more aggressive than those encountered during actual water decontamination experiments, wherein the foams were only exposed to mild magnetic stirring in the RhB solution and UV-Vis illumination during photodegradation tests. Despite the harsher conditions, the measured coating losses, ranging from 9.1 to 12.7% (Table 2), can be considered a satisfying result at the preliminary stage. Nonetheless, the trend of increasing weight loss with higher TiO_2 content might indicate that the coating becomes more brittle with an increase in the TiO_2 content.

3.2. Water decontamination

3.2.1. Adsorption and photodegradation tests

To evaluate the adsorption properties of the foams, RhB removal experiments were performed under dark conditions. Fig. 7A presents the capture ability of rGO-, rGO-TiO_2 1:1-, 1:2-, and 1:3-coated foams compared to pristine PU. The PU foams showed significant adsorption capability by removing 55% of RhB after 3.5 h, which agrees with the results reported in literature [69], [70]. Slightly higher removal efficiencies were achieved by the TiO_2-based foams (70% for rGO-TiO_2 1:1 and 1:2; 75% for rGO-TiO_2 1:3). Conversely, the rGO coating caused a reduction in the RhB adsorption properties (42% RhB removal) compared to pristine PU. The RhB adsorption mechanism, both in the case of PU and coated samples, is probably based on both electrostatic and π-π interactions, as well as on the formation of hydrogen bonds [71], [72], [73].

Experiments were also performed under UV-Vis irradiation to assess the possible improvements to the decontamination properties of the coated foams imparted by the combination of the adsorption and photodegradation phenomena. The direct RhB degradation by light was estimated through a photolysis test, and the results are shown in Fig. 7B.

Pristine PU and rGO-coated foams exhibited a similar behavior as both materials, when exposed to UV-Vis light, reached removal efficiencies (70% and 62% after 3 h, respectively) that were approximately 15% and 20%, respectively, higher than those obtained only by adsorption. As negligible photolysis phenomena were observed, the improved removal capability of PU could be ascribed to a possible alteration of the morphology of the uncoated foam under UV-Vis irradiation [74]. This is evidenced by the differences between the TG (Fig. S1) and DSC (Fig. S2) curves of pristine and illuminated PU samples. Conversely, in the case of the rGO-coated foam, the occurrence of photocatalytic events should be considered [75] as they may contribute to the enhanced removal efficiency. The other three curves, i.e., rGO-TiO_2 1:1, 1:2, and 1:3, exhibited a clear change of slope at 0 min. Indeed, after 30 min under dark conditions, with the activation of the UV-Vis lamp, the TiO_2 in the coating starts absorbing light and promoting photodegradation reactions [76], [77], [78]. All the three curves reached 100% for RhB removal after 180 min. However, Fig. 7B indicates that an increase in the TiO_2 content accelerated the decontamination process, as complete RhB removal was reached at 120 min using the rGO-TiO_2 1:2-coated foam and at 90 min using the rGO-TiO_2 1:3-coated foam. As reported in literature, the photodegradation capacity of rGO-TiO_2 materials is mainly based on the generation of $OH^{\bullet}$ and $O_2^{\bullet -}$ radicals upon light absorption [76], [79].

These findings were corroborated by kinetic analysis. Following previous studies on rGO-TiO_2 photocatalysts [80], [81], the data acquired from 0 min were interpolated with a pseudo-first order model (Fig. S5), in which the kinetic constant k (min^{-1}) represents the whole

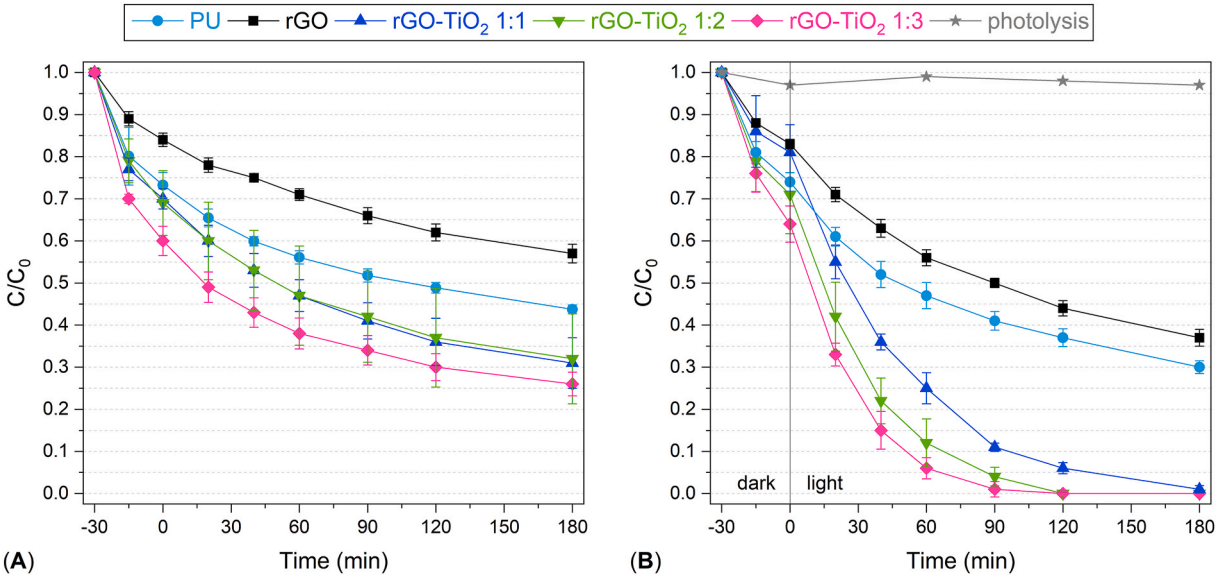

Fig. 7. Normalized concentration of RhB solution during adsorption (A) and photodegradation (B) tests.

Table 3
Decontamination kinetic constant k (min^{-1}) and R^2 values obtained from pseudo first-order kinetic modeling of experimental data for PU, rGO-, rGO-TiO_2 1:1-, 1:2-, and 1:3-coated samples in UV-Vis light conditions.

Coating	k (min^{-1})	R^2
No coating	0.0048	0.9550
rGO	0.0044	0.9679
rGO-TiO_2 1:1	0.0242	0.9928
rGO-TiO_2 1:2	0.0320	0.9964
rGO-TiO_2 1:3	0.0461	0.9844

process, accounting for both adsorption and photodegradation. This assumption derives from the Langmuir-Hinshelwood (L-H) kinetic model, commonly used to describe concurrent adsorption and heterogeneous photocatalysis processes, which can be approximated as a pseudo-first order model if the contaminant concentration is low [76], [82]. As reported in Table 3, the model fits the data related to rGO--TiO_2-coated foams extremely well, with $R^2 > 0.99$ for the 1:1- and 1:2-coated samples and $R^2 > 0.98$ for the 1:3-coated sample. Conversely, the model accuracy is lower for the other two materials, with $R^2 < 0.97$ and $R^2 < 0.96$ for rGO-coated and PU foams, respectively. In addition, there is one order of magnitude of difference between the kinetic constants of the TiO_2-containing materials (0.0242 min^{-1} for 1:1-, 0.0320 min^{-1} for 1:2-, and 0.0461 min^{-1} for 1:3-coated foams) and those of the rGO-coated (0.0044 min^{-1}) and PU (0.0048 min^{-1}) foams. These results further suggest that, under UV-Vis light, two different decontamination processes occur: i) a photocatalysis-based process, in the case of the samples coated with rGO-TiO_2, ii) an adsorption-based process, for the other two materials. Moreover, the progressive increase in k from the 1:1- to the 1:2- and 1:3-coated samples suggests that the photodegradation rate is proportional to the TiO_2 content of the material.

Considering the noticeable diversity among photoactive structured materials reported in literature and the wide variety of experimental setups, the results of this study can hardly be compared to those of previous studies. A tentative comparison with the results of Men et al. [54] and Liu et al. [55] indicates that the foams prepared in this study,

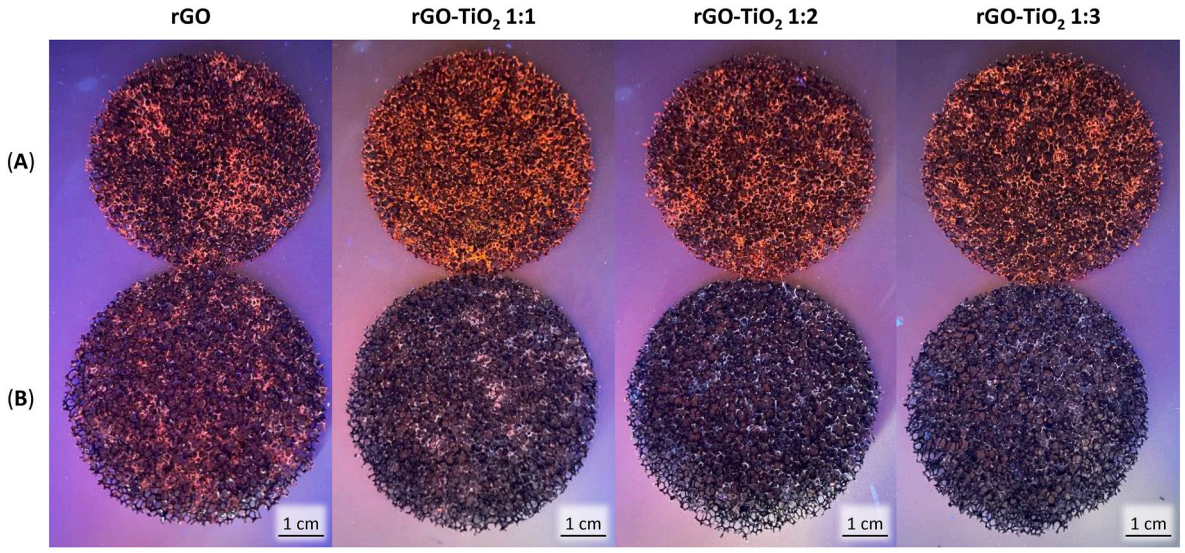

Fig. 8. Coated foams under 366 nm-centered light irradiation after adsorption (A) or photodegradation (B) tests.

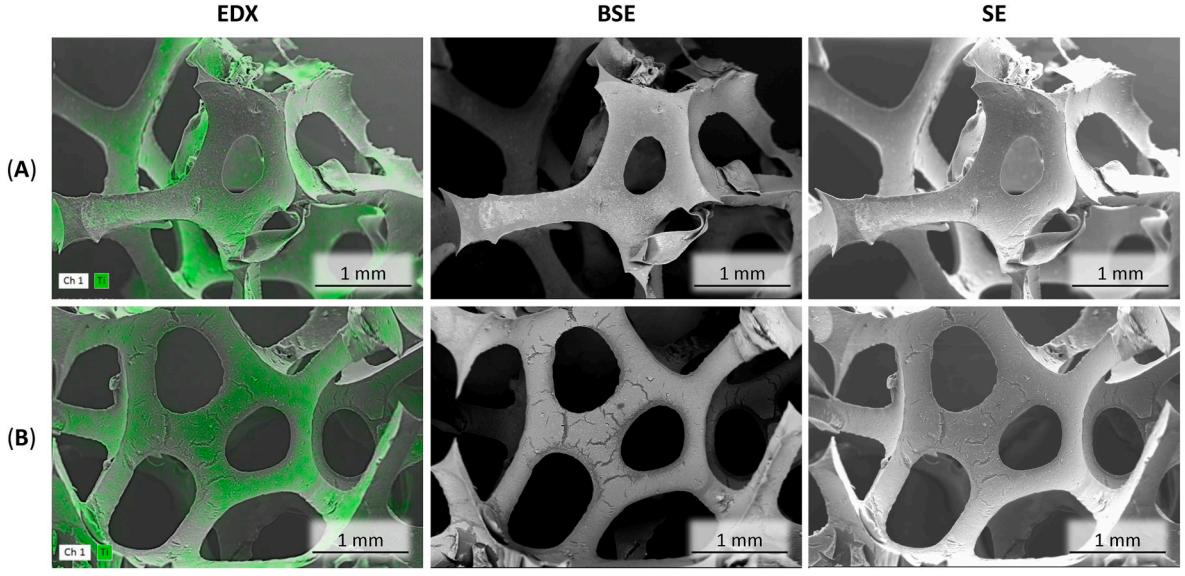

Fig. 9. SEM-EDX, backscattered electron (BSE), and secondary electron (SE) images of rGO-TiO_2 1:3-coated foams after adsorption (A) and photodegradation (B) tests at 100x magnification.

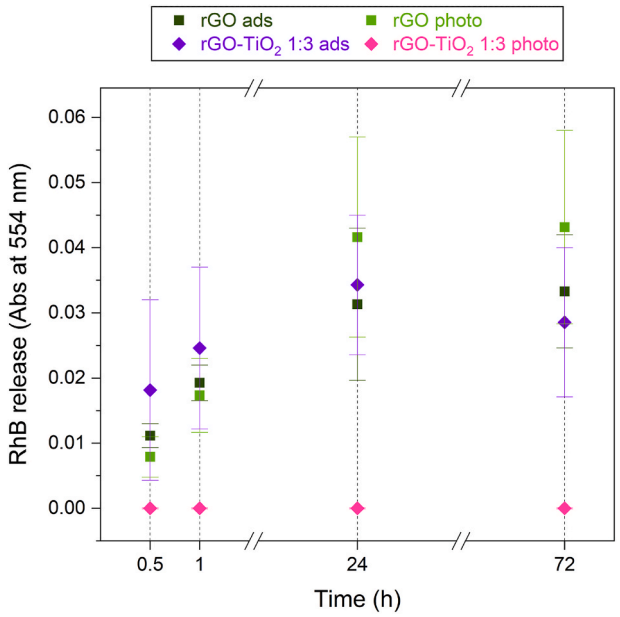

Fig. 10. Water absorbance at 554 nm after 0.5, 1, 24, and 72 h of immersion of rGO or rGO-TiO_2 1:3-coated foams after adsorption (ads) or photodegradation (photo) experiments.

although prepared using a relatively simpler process, featured a similar or even superior RhB removal performance.

At the end of decontamination experiments using rGO-TiO_2 1:3-coated foams, i.e., the specimens with the highest TiO_2 content, the Ti concentration in the treated RhB solution was measured to assess the possible leaching of TiO_2. ICP-OES analysis reported less than 2 μg L^{-1} after tests in dark and 3 ± 1 μg L^{-1} after tests under UV-Vis light. Therefore, it can be stated that no significant TiO_2 leaching occurred from rGO-TiO_2 coating.

After conducting the adsorption and photodegradation experiments, the coated foams were exposed to light at a wavelength of approximately 366 nm to reveal the possible presence of RhB through fluorescence, which causes bright pink spots to appear in the areas where RhB is present. In Fig. 8A, RhB can be clearly detected on all the foams employed in the adsorption experiments, i.e., under dark conditions, as diffused pink areas are visible on their surface. However, after the photodegradation tests (Fig. 8B), RhB was visible in large amounts only on the rGO-coated foam, which exhibited a widespread pink color. Regarding the rGO-TiO_2 coatings, limited pink areas were observed on the 1:1 samples, which completely disappeared as the TiO_2 content increased, and the rGO-TiO_2 1:2 and 1:3 specimens appeared completely black. Together with the results shown in Fig. 7, it can be hypothesized that RhB was first removed from water by adsorption on the foam surface and was successively photodegraded. Thus, after 180 min of testing, RhB could be detected on the rGO-TiO_2 1:1-coated foams, which probably exhibited slower degradation kinetics than the rGO-TiO_2 1:2 and 1:3-coated samples.

The degradation pathway of RhB is expected to unfold according to two alternative processes, as reported in the literature [83], [84], [85], [86]. The first process involves the formation of several N-de-ethylation intermediates, whereas the second process involves the destruction of the conjugated structure. These processes are followed by ring cleavage, which is fostered by the attack of photogenerated $OH^{\bullet}$ and $O_2^{\bullet-}$ radicals on the aromatic ring, and the subsequent formation of several organic acid molecules, such as oxalic, benzoic, malonic, glutaric, phthalic, succinic, and maleic acid. These species eventually undergo complete mineralization to CO_2 and H_2O.

The foams coated with rGO-TiO_2 1:3 were also characterized via SEM after the adsorption and photodegradation tests (Fig. 9). Compared to the results presented in Fig. 4, no coating detachment or significant structure alteration can be noticed here; this further confirms the promising stability of the material. Similarly, no evident changes are visible in both the TG and DSC plots of the rGO-TiO_2 1:3-coated foams after the adsorption and photodegradation experiments (Figs. S3 and S4), except for a mild decrease in the T_g of the PU substrate. However, this effect was milder than that suffered by the uncoated PU foam after its exposure to the UV-Vis lamp (Fig. S2), indicating that the coating could provide reasonable protective action.

3.2.2. *RhB and TiO_2 release analysis*

The foams coated with rGO or rGO-TiO_2 1:3, employed in water decontamination experiments, were eventually immersed for a prolonged time in dH_2O to assess the possible release of RhB or TiO_2.

For the rGO-TiO_2 1:3 samples, ICP-OES measured a Ti concentration <2 μg L^{-1}, thereby confirming a negligible TiO_2 release from the rGO-TiO_2 1:3-coated foams not only after being used in both types of decontamination tests but also after a prolonged immersion in dH_2O.

Fig. 10 and S6 show that the rGO-coated foams, after both adsorption and photodegradation tests, were responsible for a slight water contamination with RhB, which reached a plateau at 24 h. This result is consistent with the release of RhB observed on the foam surface (Fig. 8). However, the amount of dye detected in water was remarkably lower than that previously removed, with absorbance values one order of magnitude lower than those of the initial 3 ppm RhB solution, i.e., approximately 0.75 (Fig. S6). This suggests that, once adsorbed by the foams, the dye is not easily released, confirming the good decontamination ability of these materials. These considerations can be extended to the rGO-TiO_2 1:3-coated samples used in adsorption experiments, which exhibited the presence of RhB on their surface (Fig. 8A). Moreover, the slight decrease in absorbance at 72 h may suggest the occurrence of partial re-adsorption phenomena, which could mitigate the initial release and confirm the tendency of RhB to remain on the foam surface. Contrarily, the rGO-TiO_2 1:3-coated foam exposed to the lamp did not release RhB even after 72 h, confirming its absence on the foam surface (Fig. 8B). This result represents a further confirmation of the photodegradation ability of the TiO_2-containing coatings developed in this work.

4. Conclusions

This study proposed and demonstrated an innovative low-tech and low-energy consuming strategy to immobilize TiO_2 nanoparticles and rGO on the surface of 3D floating polyurethane foams. The prepared slurries were deposited at room temperature through a dip-coating process, followed by blowing compressed air and final material consolidation at 40 °C. The coating formulation only consisted of GO aqueous dispersion, TiO_2 nanoparticles (in GO:TiO_2 ratio of 1:1, 1:2, or 1:3), and L-ascorbic acid and did not contain an additional binder. TiO_2 incorporation in the coating layer was achieved by exploiting the self-assembling properties of rGO.

The coated foams exhibited both adsorption and UV-Vis photodegradation capabilities toward the dye RhB because of the concurrent presence of PU, rGO, and TiO_2. In particular, foams coated with the highest TiO_2 amount (i.e., rGO:TiO_2 = 1:3) showed the highest RhB removal performance, reaching complete decontamination after 90 min of exposure to UV-Vis light, as evidenced via foam characterization and the RhB release experiments. The proposed materials are particularly interesting considering their photoactivity combined with easy handling, facile preparation and use, as well as simple retrieval from the treated solutions.

CRediT authorship contribution statement

Anna Dotti: Writing – original draft, Visualization, Methodology, Investigation, Formal analysis, Data curation. **Andrea Basso Peressut:**

Writing – original draft, Visualization, Validation, Methodology, Formal analysis, Data curation. **Lorenzo Viganò:** Writing – review & editing, Visualization, Validation, Methodology, Formal analysis. **Barbara Di Credico:** Writing – review & editing, Visualization, Validation, Supervision, Methodology. **Roberto Matarrese:** Writing – review & editing, Validation, Supervision, Resources, Methodology. **Saverio Latorrata:** Writing – review & editing, Validation, Supervision, Resources, Methodology, Conceptualization.

Declaration of competing interest

The authors declare that they have no known competing financial interests or personal relationships that could have appeared to influence the work reported in this paper.

Acknowledgments

The authors acknowledge the financial support provided by the Italian Ministry of University and Research (MUR) within the framework of the PRIN project "Sustainable design of composite materials for hybrid wastewater treatment – SMARTER" – CUP: D53C24003760001. Roberto Matarrese acknowledges the support from Project RESELECT under the PNRR call for Mission 4, Component 2, Investment 1.1, funded by European Union – NextGenerationEU – CUP: D53D23004080006; MUR code: 2022SRFZTJ.

Appendix A. Supplementary data

Supplementary data to this article can be found online at https://doi.org/10.1016/j.mtchem.2026.103611.

Data availability

Data will be made available on request.

References

[1] R. Rashid, I. Shafiq, P. Akhter, M.J. Iqbal, M. Hussain, A state-of-the-art review on wastewater treatment techniques: the effectiveness of adsorption method, Environ. Sci. Pollut. Control Ser. 28 (8) (Jan. 2021) 9050–9066, https://doi.org/10.1007/S11356-021-12395-X.

[2] M. Ahtasham Iqbal, et al., Advanced photocatalysis as a viable and sustainable wastewater treatment process: a comprehensive review, Environ. Res. 253 (Jul. 2024) 118947, https://doi.org/10.1016/J.ENVRES.2024.118947, 1–30.

[3] A. Fujishima, T.N. Rao, D.A. Tryk, Titanium dioxide photocatalysis, J. Photochem. Photobiol. C Photochem. Rev. 1 (1) (Jun. 2000) 1–21, https://doi.org/10.1016/S1389-5567(00)00002-2.

[4] B. Di Credico, et al., Efficacy of the reactive oxygen species generated by immobilized TiO_2 in the photocatalytic degradation of diclofenac, Int. J. Photoenergy 2015 (1) (Jan. 2015) 919217, https://doi.org/10.1155/2015/919217, 1–13.

[5] B. Di Credico, et al., Step-by-step growth of HKUST-1 on functionalized TiO_2 surface: an efficient material for CO_2 capture and solar photoreduction, Catalysts 8 (9) (Aug. 2018) 353, https://doi.org/10.3390/CATAL8090353, 1–20.

[6] S.Y. Lee, S.J. Park, TiO_2 photocatalyst for water treatment applications, J. Ind. Eng. Chem. 19 (6) (Nov. 2013) 1761–1769, https://doi.org/10.1016/J.JIEC.2013.07.012.

[7] H. Dong, et al., An overview on limitations of TiO_2-based particles for photocatalytic degradation of organic pollutants and the corresponding countermeasures, Water Res. 79 (Aug. 2015) 128–146, https://doi.org/10.1016/J.WATRES.2015.04.038.

[8] H. Zhou, et al., MXene-derived TiO_2/MXene-loaded Ag for the degradation of the methyl orange, J. Mater. Res. 36 (Dec. 2021) 5001–5012, https://doi.org/10.1557/s43578-021-00428-7.

[9] S. Mishra, B. Sundaram, A review of the photocatalysis process used for wastewater treatment, Mater. Today Proc. 102 (Jul. 2023) 393–409, https://doi.org/10.1016/J.MATPR.2023.07.147.

[10] J.A. Rengifo-Herrera, C. Pulgarin, Why five decades of massive research on heterogeneous photocatalysis, especially on TiO_2, has not yet driven to water disinfection and detoxification applications? Critical review of drawbacks and challenges, Chem. Eng. J. 477 (Dec. 2023) 146875, https://doi.org/10.1016/J.CEJ.2023.146875, 1–16.

[11] M. Muscetta, P. Ganguly, L. Clarizia, Solar-powered photocatalysis in water purification: applications and commercialization challenges, J. Environ. Chem. Eng. 12 (3) (Jun. 2024) 113073, https://doi.org/10.1016/J.JECE.2024.113073, 1–18.

[12] V. Nogueira, et al., Assessing the ecotoxicity of metal nano-oxides with potential for wastewater treatment, Environ. Sci. Pollut. Control Ser. 22 (May 2015) 13212–13224, https://doi.org/10.1007/s11356-015-4581-9.

[13] R. Giovannetti, E. Rommozzi, M. Zannotti, C.A. D'Amato, Recent advances in graphene based TiO_2 nanocomposites ($GTiO_2Ns$) for photocatalytic degradation of synthetic dyes, Catalysts 7 (10) (Oct. 2017) 305, https://doi.org/10.3390/CATAL7100305, 1–34.

[14] M. Kocijan, L. Curkovic, G. Gonçalves, M. Podlogar, The potential of rGO@TiO_2 photocatalyst for the degradation of organic pollutants in water, Sustainability 14 (19) (Oct. 2022) 12703, https://doi.org/10.3390/SU141912703, 1–19.

[15] J.J. Shao, W. Lv, Q.H. Yang, Self-assembly of graphene oxide at interfaces, Adv. Mater. 26 (32) (Aug. 2014) 5586–5612, https://doi.org/10.1002/ADMA.201400267.

[16] A. Basso Peressut, et al., Reduced graphene oxide/waste-derived TiO_2 composite membranes: preliminary: study of a new material for hybrid wastewater treatment, Nanomaterials 13 (6) (Mar. 2023) 1–21, https://doi.org/10.3390/nano13061043.

[17] S. Latorrata, et al., Reduced graphene oxide membranes as potential self-assembling filter for wastewater treatment, Minerals 11 (1) (Jan. 2021) 1–16, https://doi.org/10.3390/min11010015.

[18] J. Wang, B. Chen, Adsorption and coadsorption of organic pollutants and a heavy metal by graphene oxide and reduced graphene materials, Chem. Eng. J. 281 (Dec. 2015) 379–388, https://doi.org/10.1016/J.CEJ.2015.06.102.

[19] N. Yahya, et al., A review of integrated photocatalyst adsorbents for wastewater treatment, J. Environ. Chem. Eng. 6 (6) (Dec. 2018) 7411–7425, https://doi.org/10.1016/j.jece.2018.06.051.

[20] Q. Dai, et al., The MIL-125(Ti)/Co_3O_4 towards efficiently removing tetracycline by synergistic adsorption-photocatalysis roles, Mater. Des. 250 (Feb. 2025) 113608, https://doi.org/10.1016/J.MATDES.2025.113608, 1–11.

[21] G. Luna-Sanguino, et al., Solar photocatalytic degradation of pesticides over TiO_2-rGO nanocomposites at pilot plant scale, Sci. Total Environ. 737 (Oct. 2020) 140286, https://doi.org/10.1016/J.SCITOTENV.2020.140286, 1–10.

[22] A. Tayel, A.R. Ramadan, O.A. El Seoud, Titanium dioxide/graphene and titanium dioxide/graphene oxide nanocomposites: synthesis, characterization and photocatalytic applications for water decontamination, Catalysts 8 (11) (Oct. 2018) 491, https://doi.org/10.3390/CATAL8110491, 1–45.

[23] I. Tismanar, A.C. Obreja, O. Buiu, A. Duta, VIS-active TiO_2–graphene oxide composite thin films for photocatalytic applications, Appl. Surf. Sci. 538 (Feb. 2021) 147833, https://doi.org/10.1016/J.APSUSC.2020.147833, 1–12.

[24] Y. Chen, X. Dong, Y. Cao, J. Xiang, H. Gao, Enhanced photocatalytic activities of low-bandgap TiO_2-reduced graphene oxide nanocomposites, J. Nanoparticle Res. 19 (200) (Jun. 2017) 1–13, https://doi.org/10.1007/s11051-017-3871-1.

[25] M. Minella, F. Sordello, C. Minero, Photocatalytic process in TiO_2/graphene hybrid materials. Evidence of charge separation by electron transfer from reduced graphene oxide to TiO_2, Catal. Today 281 (Mar. 2017) 29–37, https://doi.org/10.1016/J.CATTOD.2016.03.040.

[26] E. Kusiak-Nejman, A.W. Morawski, TiO_2/graphene-based nanocomposites for water treatment: a brief overview of charge carrier transfer, antimicrobial and photocatalytic performance, Appl. Catal. B Environ. 253 (Sep. 2019) 179–186, https://doi.org/10.1016/J.APCATB.2019.04.055.

[27] N.M. El-Shafai, M.E. El-Khouly, M. El-Kemary, M.S. Ramadan, A.S. Derbalah, M. S. Masoud, Fabrication and characterization of graphene oxide–titanium dioxide nanocomposite for degradation of some toxic insecticides, J. Ind. Eng. Chem. 69 (Jan. 2019) 315–323, https://doi.org/10.1016/J.JIEC.2018.09.045.

[28] M. Sohail, et al., Synthesis of well-dispersed TiO_2@reduced graphene oxide (rGO) nanocomposites and their photocatalytic properties, Mater. Res. Bull. 90 (Jun. 2017) 125–130, https://doi.org/10.1016/J.MATERRESBULL.2017.02.025.

[29] L. Jing, H.L. Tan, R. Amal, Y.H. Ng, K.N. Sun, Polyurethane sponge facilitating highly dispersed TiO_2 nanoparticles on reduced graphene oxide sheets for enhanced photoelectro-oxidation of ethanol, J. Mater. Chem. A 3 (30) (Jul. 2015) 15675–15682, https://doi.org/10.1039/C5TA04203H.

[30] Y. Gao, M. Hu, B. Mi, Membrane surface modification with TiO_2–graphene oxide for enhanced photocatalytic performance, J. Membr. Sci. 455 (Apr. 2014) 349–356, https://doi.org/10.1016/J.MEMSCI.2014.01.011.

[31] R. Liu, et al., Reduced graphene oxide/TiO_2(B) immobilized on nylon membrane with enhanced photocatalytic performance, Sci. Total Environ. 799 (Dec. 2021) 149370, https://doi.org/10.1016/J.SCITOTENV.2021.149370, 1–10.

[32] H. Abadikhah, et al., High flux thin film nanocomposite membrane incorporated with functionalized TiO_2@reduced graphene oxide nanohybrids for organic solvent nanofiltration, Chem. Eng. Sci. 204 (Aug. 2019) 99–109, https://doi.org/10.1016/J.CES.2019.04.022.

[33] S.P. Sundaran, C.R. Reshmi, P. Sagitha, A. Sujith, Polyurethane nanofibrous membranes decorated with reduced graphene oxide–TiO_2 for photocatalytic templates in water purification, J. Mater. Sci. 55 (14) (May 2020) 5892–5907, https://doi.org/10.1007/s10853-020-04414-y.

[34] A.K. Nair, J.B. Jagadeesh, TiO_2 nanosheet-graphene oxide based photocatalytic hierarchical membrane for water purification, Surf. Coating. Technol. 320 (Jun. 2017) 259–262, https://doi.org/10.1016/J.SURFCOAT.2017.01.022.

[35] M. Kocijan, et al., Immobilised rGO/TiO_2 nanocomposite for multi-cycle removal of Methylene blue dye from an aqueous medium, Appl. Sci. 12 (1) (Jan. 2022) 1–14, https://doi.org/10.3390/app12010385.

[36] M. Olak-Kucharczyk, G. Szczepanska, M.H. Kudzin, M. Pisarek, The photocatalytical properties of RGO/TiO_2 coated fabrics, Coatings 10 (2020) 1041, https://doi.org/10.3390/coatings10111041, 1–15.

[37] C.P. Athanasekou, et al., Prototype composite membranes of partially reduced graphene oxide/TiO_2 for photocatalytic ultrafiltration water treatment under visible light, Appl. Catal. B Environ. 158 (159) (Oct. 2014) 361–372, https://doi.org/10.1016/J.APCATB.2014.04.012.

[38] L. Lin, H. Wang, P. Xu, Immobilized TiO_2-reduced graphene oxide nanocomposites on optical fibers as high performance photocatalysts for degradation of pharmaceuticals, Chem. Eng. J. 310 (Feb. 2017) 389–398, https://doi.org/10.1016/J.CEJ.2016.04.024.

[39] J. Zhou, Y. Zhang, G. Jia, Z. Chen, Y. Yang, L. Zhang, A multifunctional sponge incorporated with TiO_2 and graphene oxide as a reusable absorbent for oil/water separation and dye absorption, New J. Chem. 45 (10) (Mar. 2021) 4835–4842, https://doi.org/10.1039/D0NJ06298G.

[40] C. Teodosiu, R. Wenkert, L. Tofan, C. Paduraru, Advances in preconcentration/removal of environmentally relevant heavy metal ions from water and wastewater by sorbents based on polyurethane foam, Rev. Chem. Eng. 30 (4) (Aug. 2014) 403–420, https://doi.org/10.1515/REVCE-2013-0036.

[41] H. Zhu, et al., A versatile and cost-effective reduced graphene oxide-crosslinked polyurethane sponge for highly effective wastewater treatment, RSC Adv. 6 (Mar. 2016) 38350–38355, https://doi.org/10.1039/c6ra05450a.

[42] C. Xia, Y. Li, T. Fei, W. Gong, Facile one-pot synthesis of superhydrophobic reduced graphene oxide-coated polyurethane sponge at the presence of ethanol for oil-water separation, Chem. Eng. J. 345 (Aug. 2018) 648–658, https://doi.org/10.1016/J.CEJ.2018.01.079.

[43] Y. Liu, et al., Cost-effective reduced graphene oxide-coated polyurethane sponge as a highly efficient and reusable oil-absorbent, ACS Appl. Mater. Interfaces 5 (20) (Oct. 2013) 10018–10026, https://doi.org/10.1021/AM4024252.

[44] R. Balzarotti, A. Migliavacca, A. Basso Peressut, A. Mansutti, S. Latorrata, A novel approach to water softening based on graphene oxide-activated open cell foams, C-Journal of Carbon Research 9 (1) (Mar. 2023) 1–10, https://doi.org/10.3390/c9010006.

[45] N. Davari, E. Falletta, C.L. Bianchi, V. Yargeau, D.C. Boffito, TiO_2 nanotubes immobilized on polyurethane foam as a floating photocatalyst for water treatment, Catal. Today 436 (Jun. 2024) 114725, https://doi.org/10.1016/J.CATTOD.2024.114725, 1–16.

[46] L. Li, Y. Li, H. Xu, W. Zhang, Novel floating TiO_2 photocatalysts for polluted water decontamination based on polyurethane composite foam, Separ. Sci. Technol. 50 (2) (Jan. 2015) 164–173, https://doi.org/10.1080/01496395.2014.949773.

[47] P. Augusto, et al., Green polyurethane foam coated with a copolymer containing TiO_2 nanoparticles through non-solvent induced phase separation: a photocatalytic water cleaning approach, J. Appl. Polym. Sci. 142 (19) (Feb. 2025) e56869, https://doi.org/10.1002/APP.56869, 1–16.

[48] S.W. Lee, S. Obregón-Alfaro, V. Rodríguez-González, Photocatalytic coatings of silver–TiO_2 nanocomposites on foamed waste-glass prepared by sonochemical process, J. Photochem. Photobiol. Chem. 221 (1) (Jun. 2011) 71–76, https://doi.org/10.1016/J.JPHOTOCHEM.2011.04.026.

[49] E. Valadez-Renteria, J. Oliva, V. Rodriguez-Gonzalez, Photocatalytic materials immobilized on recycled supports and their role in the degradation of water contaminants: a timely review, Sci. Total Environ. 807 (Feb. 2022) 150820, https://doi.org/10.1016/J.SCITOTENV.2021.150820, 1–16.

[50] Q. Wei, O. Oribayo, X. Feng, G.L. Rempel, Q. Pan, Synthesis of polyurethane foams loaded with TiO_2 nanoparticles and their modification for enhanced performance in oil spill cleanup, Ind. Eng. Chem. Res. 57 (27) (Jul. 2018) 8918–8926, https://doi.org/10.1021/ACS.IECR.8B01037.

[51] G. Chen, et al., Improvement of self-cleaning waterborne polyurethane-acrylate with cationic TiO_2/reduced graphene oxide, RSC Adv. 9 (32) (Jun. 2019) 18652–18662, https://doi.org/10.1039/C9RA03250A.

[52] L. Ni, Y. Li, C. Zhang, L. Li, W. Zhang, D. Wang, Novel floating photocatalysts based on polyurethane composite foams modified with silver/titanium dioxide/graphene ternary nanoparticles for the visible-light-mediated remediation of diesel-polluted surface water, J. Appl. Polym. Sci. 133 (19) (May 2016) 43400, https://doi.org/10.1002/APP.43400, 1–9.

[53] C. Wang, Z. hai Shi, L. Peng, W. min He, B. liang Li, K. zhi Li, Preparation of carbon foam-loaded nano-TiO_2photocatalyst and its degradation on methyl orange, Surf. Interfaces 7 (Jun. 2017) 116–124, https://doi.org/10.1016/J.SURFIN.2017.03.007.

[54] X. Men, et al., Facile fabrication of TiO_2/graphene composite foams with enhanced photocatalytic properties, J. Alloys Compd. 703 (May 2017) 251–257, https://doi.org/10.1016/J.JALLCOM.2017.01.353.

[55] T. Liu, S. Sun, L. Zhou, P. Li, Z. Su, G. Wei, Polyurethane-supported graphene oxide foam functionalized with carbon dots and TiO_2 particles for photocatalytic degradation of dyes, Appl. Sci. 9 (2) (Jan. 2019) 293, https://doi.org/10.3390/APP9020293, 1–11.

[56] W. Wang, Z. Wang, J. Liu, Z. Zhang, L. Sun, Single-step one-pot synthesis of graphene foam/TiO_2 nanosheet hybrids for effective water treatment, Sci. Rep. 7 (1) (Mar. 2017) 1–8, https://doi.org/10.1038/SREP43755.

[57] M. Abouri, et al., Enhanced photocatalytic degradation of Rhodamine B using polyaniline-coated $XTiO_3$(X = Co, Ni) nanocomposites, Sci. Rep. 15 (1) (Jan. 2025) 1–16, https://doi.org/10.1038/s41598-024-83610-1.

[58] UNI 11259, UNI Ente Italiano Di Normazione, 2008.

[59] Z. Chen, et al., C, F co-doping Ag/TiO_2 with visible light photocatalytic performance toward degrading Rhodamine B, Environ. Res. 232 (Sep. 2023) 116311, https://doi.org/10.1016/J.ENVRES.2023.116311, 1–14.

[60] D. Filip, D. Macocinschi, S. Vlad, Thermogravimetric study for polyurethane materials for biomedical applications, Compos. B Eng. 42 (6) (Sep. 2011) 1474–1479, https://doi.org/10.1016/J.COMPOSITESB.2011.04.050.

[61] A. Mohammadi, M. Barikani, M. Barmar, Synthesis and investigation of thermal and mechanical properties of *in situ* prepared biocompatible Fe_3O_4/polyurethane elastomer nanocomposites, Polym. Bull. 72 (Nov. 2014) 219–234, https://doi.org/10.1007/s00289-014-1268-1.

[62] F. Askari, M. Barikani, M. Barmar, F. Shokrolahi, M. Vafayan, Study of thermal stability and degradation kinetics of polyurethane-ureas by thermogravimetry, Iran. Polym. J. (Engl. Ed.) 24 (Aug. 2015) 783–789, https://doi.org/10.1007/s13726-015-0367-7.

[63] I. Ristić, S. Cakić, N. Vukić, V. Teofilović, J. Tanasić, B. Pilić, The influence of soft segment structure on the properties of polyurethanes, Polymers 15 (18) (Sep. 2023) 3755, https://doi.org/10.3390/POLYM15183755, 1–14.

[64] H. Lu, P. Sun, Z. Zheng, X. Yao, X. Wang, F.C. Chang, Reduction-sensitive rapid degradable poly(urethane-urea)s based on cystine, Polym. Degrad. Stabil. 97 (4) (Apr. 2012) 661–669, https://doi.org/10.1016/J.POLYMDEGRADSTAB.2011.12.023.

[65] T.K. Chen, J.Y. Chui, T.S. Shieh, Glass transition behaviors of a polyurethane hard segment based on 4,4'-Diisocyanatodiphenylmethane and 1,4-Butanediol and the calculation of microdomain composition, Macromolecules 30 (17) (Aug. 1997) 5068–5074, https://doi.org/10.1021/MA9618639.

[66] H. Hatakeyama, H. Matsumura, T. Hatakeyama, Glass transition and thermal degradation of rigid polyurethane foams derived from castor oil-molasses polyols, J. Therm. Anal. Calorim. 111 (Jul. 2012) 1545–1552, https://doi.org/10.1007/s10973-012-2501-5.

[67] J.K. Njuguna, P. Muchiri, N.W. Karuri, M. Herzog, K. Dimitrov, F.M. Mwema, Determination of thermo-mechanical properties of recycled polyurethane from glycolysis polyol, Sci. Afr. 12 (Jul. 2021) 1–10, https://doi.org/10.1016/J.SCIAF.2021.E00755, e00755.

[68] R. Suriano, A. Mantelli, G. Griffini, S. Turri, G. Bonaiti, Styrene-free liquid resins for composite reformulation, in: Systemic Circular Economy Solutions for Fiber Reinforced Composites, Jan. 2023, pp. 99–123, https://doi.org/10.1007/978-3-031-22352-5_6.

[69] J. Zhao, et al., Zr-MOFs loaded on polyurethane foam by polydopamine for enhanced dye adsorption, Journal of Environmental Sciences 101 (Mar. 2021) 177–188, https://doi.org/10.1016/J.JES.2020.08.021.

[70] R. Kumar, P. Kumar, S. Panigrahi, N. Lakshminarasimhan, R. Shunmugam, Efficient removal of rhodamine B and methylene blue from water using polyurethane based porous material, Polym. Eng. Sci. 62 (12) (Dec. 2022) 4082–4089, https://doi.org/10.1002/PEN.26168.

[71] A. Chandrashekar, S. Vargheese, J.G. Vijayan, J.A. Gopi, T.N. Prabhu, Highly efficient removal of rhodamine B dye using nanocomposites made from cotton seed oil-based polyurethane and silylated nanocellulose, J. Polym. Environ. 30 (12) (Sep. 2022) 4999–5011, https://doi.org/10.1007/s10924-022-02567-2.

[72] U. Jinendra, D. Bilehal, B.M. Nagabhushana, A.P. Kumar, Adsorptive removal of Rhodamine B dye from aqueous solution by using graphene–based nickel nanocomposite, Heliyon 7 (4) (Apr. 2021) e06851, https://doi.org/10.1016/j.heliyon.2021.e06851, 1–9.

[73] J. Sahar, A. Naeem, M. Farooq, S. Zareen, A. Urrahman, Thermodynamic studies of adsorption of rhodamine B and Congo red on graphene oxide, Desalination Water Treat. 164 (Oct. 2019) 228–239, https://doi.org/10.5004/dwt.2019.24436.

[74] D. Rosu, L. Rosu, C.N. Cascaval, IR-change and yellowing of polyurethane as a result of UV irradiation, Polym. Degrad. Stabil. 94 (4) (Apr. 2009) 591–596, https://doi.org/10.1016/J.POLYMDEGRADSTAB.2009.01.013.

[75] V.L.E. Siong, X.H. Tai, K.M. Lee, J.C. Juan, C.W. Lai, Unveiling the enhanced photoelectrochemical and photocatalytic properties of reduced graphene oxide for photodegradation of methylene blue dye, RSC Adv. 10 (62) (Oct. 2020) 37905–37915, https://doi.org/10.1039/D0RA06703B.

[76] X. Zhou, S. Zhou, F. Ma, Y. Xu, Synergistic effects and kinetics of rGO-modified TiO_2 nanocomposite on adsorption and photocatalytic degradation of humic acid, J. Environ. Manag. 235 (Apr. 2019) 293–302, https://doi.org/10.1016/J.JENVMAN.2019.01.026.

[77] F. Wang, K. Zhang, Reduced graphene oxide-TiO_2 nanocomposite with high photocatalytic activity for the degradation of rhodamine B, J. Mol. Catal. Chem. 345 (1–2) (Jul. 2011) 101–107, https://doi.org/10.1016/j.molcata.2011.05.026.

[78] Á. Tolosana-Moranchel, A. Manassero, M.L. Satuf, O.M. Alfano, J.A. Casas, A. Bahamonde, Influence of TiO_2-rGO optical properties on the photocatalytic activity and efficiency to photodegrade an emerging pollutant, Appl. Catal. B Environ. 246 (Jun. 2019) 1–11, https://doi.org/10.1016/j.apcatb.2019.01.054.

[79] A. Tolosana-Moranchel, et al., Nature and photoreactivity of TiO_2-rGO nanocomposites in aqueous suspensions under UV-A irradiation, Appl. Catal. B Environ. 241 (21) (Feb. 2019) 375–384, https://doi.org/10.1016/j.apcatb.2018.09.070.

[80] Q. Khan, M. Sayed, I. Gul, Titania/reduced graphene oxide nanocomposites (TiO_2/rGO) as an efficient photocatalyst for the effective degradation of brilliant green in aqueous media: effect of peroxymonosulfate and operational parameters, Environ. Sci. Pollut. Control Ser. 30 (27) (May 2023) 71025–71047, https://doi.org/10.1007/s11356-023-27316-3.

[81] L.-J. Luo, et al., Photocatalytic degradation of bisphenol A by TiO_2-reduced graphene oxide nanocomposites, React. Kinet. Mech. Catal. 114 (1) (Aug. 2014) 311–322, https://doi.org/10.1007/s11144-014-0761-8.

[82] K. Vasanth Kumar, K. Porkodi, F. Rocha, Langmuir–Hinshelwood kinetics – a theoretical study, Catal. Commun. 9 (1) (Jan. 2008) 82–84, https://doi.org/10.1016/j.catcom.2007.05.019.

[83] F. Dalanta, H. Widiyandari, C.W. Kartikowati, A.F. Arif, A.M.I. Filardli, O. Arutanti, Green-synthesized Schottky junction Ni-TiOx suboxide photocatalyst enriched with oxygen vacancies for solar-driven degradation of emerging contaminants, Journal

of Water Process Engineering 77 (Sep. 2025) 108446, https://doi.org/10.1016/J.JWPE.2025.108446, 1–25.

[84] C.H. Nguyen, M.L. Tran, T.T. Van Tran, R.S. Juang, Enhanced removal of various dyes from aqueous solutions by UV and simulated solar photocatalysis over TiO_2/ZnO/rGO composites, Separation and Purification Technology 232 (Feb. 2020) 115962, https://doi.org/10.1016/J.SEPPUR.2019.115962, 1–14.

[85] Y. Zhao, C. Li, X. Liu, F. Gu, H.L. Du, L. Shi, Zn-doped TiO_2 nanoparticles with high photocatalytic activity synthesized by hydrogen–oxygen diffusion flame, Appl. Catal. B Environ. 79 (3) (Mar. 2008) 208–215, https://doi.org/10.1016/J.APCATB.2007.09.044.

[86] Z. He, S. Yang, Y. Ju, C. Sun, Microwave photocatalytic degradation of Rhodamine B using TiO_2 supported on activated carbon: mechanism implication, Journal of Environmental Sciences 21 (2) (Jan. 2009) 268–272, https://doi.org/10.1016/S1001-0742(08)62262-7.